CaMn_{2}Al_{10}: Itinerant Mn magnetism on the verge of magnetic order

L. Steinke, J. W. Simonson, W.-G. Yin, G. J. Smith, J. J. Kistner-Morris, S. Zellman, A. Puri, and M. C. Aronson

Phys. Rev. B **92**, 020413 — Published 24 July 2015

DOI: 10.1103/PhysRevB.92.020413

$CaMn_2Al_{10}$: itinerant Mn magnetism on the verge of magnetic order

L. Steinke[1,2⋆], J. W. Simonson[3], W.-G. Yin[1], G. J. Smith[2], J. J. Kistner-Morris[2], S. Zellman[2], A. Puri[2], and M. C. Aronson[1,2]

[1] *Condensed Matter Physics and Materials Science Department, Brookhaven National Laboratory, Upton, New York 11973, USA*

[2] *Department of Physics and Astronomy, Stony Brook University, Stony Brook, New York 11794, USA*

[3] *Department of Physics, Farmingdale State College, Farmingdale, New York 11735, USA*

(Dated: June 10, 2015)

We report the discovery of $CaMn_2Al_{10}$, a metal with strong magnetic anisotropy and moderate electronic correlations. Magnetization measurements find a CW moment of $0.83\,\mu_B$/Mn, significantly reduced from the Hund's rule value, and the magnetic entropy obtained from specific heat measurements is correspondingly small, only ≈ 9 % of $R\ln 2$. These results imply that the Mn magnetism is highly itinerant, a conclusion supported by density functional theory calculations that find strong Mn-Al hybridization. Consistent with the layered nature of the crystal structure, the magnetic susceptibility χ is anisotropic below 20 K, with a maximum ratio of $\chi_{[010]}/\chi_{[001]} \approx 3.5$. A strong power-law divergence $\chi(T) \sim T^{-1.2}$ below 20 K implies incipient ferromagnetic order with a low Curie temperature $T_C < 2$ K. Our experiments indicate that $CaMn_2Al_{10}$ is a rare example of a system where the weak and itinerant Mn-based magnetism is poised on the verge of order.

Manganese compounds are generally marked by their strong magnetic character, which is the consequence of Hund's coupling[1]. For instance, the complex crystal structure and phase diagram of elemental Mn results from competing tendencies to maximize the magnetic moment according to Hund's rule coupling and to maximize the metallic bond strength, where shorter Mn-Mn distances are energetically favorable but tend to quench the magnetism[2,3]. If the effective Coulomb interactions are sufficiently strong, Mn compounds can be robust insulators like the manganites or the Mn pnictides LaMnPO[4,5], $CaMn_2Sb_2$[6,7], and $BaMn_2As_2$[8]. Even in metallic hosts, the Mn moments can be weakly hybridized, leading to the pronounced magnetic character of systems like MnX (X = P,As,Sb,Bi)[9–12], MnB_{13}, and RMn_2X_2 (R = La,Lu,Y; X = Si,Ge)[14–16]. There are very few compounds where Mn moments are so strongly hybridized with the conduction electrons that a much reduced moment results from correlations. Examples of this rare class are metallic MnSi[17], YMn_2[18], and $HfMnGa_2$[19], where the electronic fluctuations are so strong that there is no definite moment or valence state. Here, the moment results from correlations in a fully delocalized electronic medium, and magnetic order ensues from a collective instability of the Fermi surface, either a ferromagnetic (FM) Stoner instability[20] or an antiferromagnetic (AFM) spin density wave[21]. When the ordering temperature approaches 0 K, spin fluctuations with pronounced quantum character play an increasing role in measured quantities[22,23]. Magnetic systems in this extreme limit can host a number of intriguing phenomena, from non-Fermi-liquid-behavior to emergent collective phases like magnetically mediated superconductivity[24].

The scarcity of itinerant systems with weak magnetic order has limited progress towards understanding the role of these quantum critical fluctuations in stabilizing exotic ground states. Most itinerant FM have very high Curie temperatures T_C, and there is only a handful of special

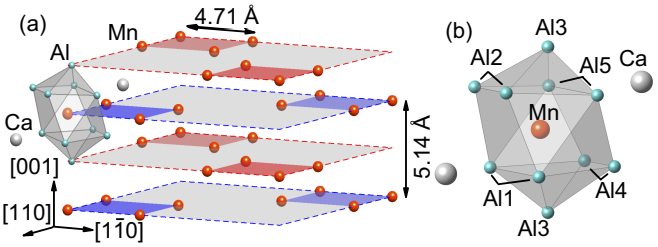

Figure 1. (Color online) (a) A simplified picture of the crystal structure of $CaMn_2Al_{10}$ that shows only the Mn lattice. Square plaquettes of Mn atoms (red) form in two planes (red and blue) separated by a distance of $c/2$ along the [001] direction. (b) The coordination polyhedron of Mn (red) with Al (teal) and Ca (gray) as indicated.

systems, like Sc_3In[25] URhGe[26], UGe_2[27], Ni_3Al[28], and $ZrZn_2$[29–31] where T_C is small enough to be tuned to zero by an external variable like doping, pressure, or magnetic field, forming a possible quantum critical point (QCP) T_C=0. In clean itinerant FM, such a QCP is generally pre-empted by a first-order transition[32], as demonstrated in pressure- and doping-dependent studies of MnSi[33] and $ZrZn_2$[34]. However, there is mounting evidence that continuous T_C=0 phase transitions can be realized in clean systems like YFe_2Al_{10}[35] and $YbNi_4P_2$[36,37], where low dimensionality apparently enhances the strength of quantum fluctuations. The discovery of new itinerant magnets with small ordering temperatures that can be tuned to instability at a QCP would be transformative, especially if they also foster unconventional superconductivity as in UGe_2[27], URhGe[26], UIr[38], and UCoGe[39].

Here, we report the discovery of $CaMn_2Al_{10}$, which could potentially fulfill these needs for both new low-dimensional magnetic systems with strong quantum fluctuations and for itinerant magnets with low ordering temperatures. $CaMn_2Al_{10}$ is a metallic compound with a

small fluctuating Mn moment. At low temperatures, the magnetization is strongly anisotropic, evidencing a pronounced quasi two-dimensional (2D) character. The ac susceptibility χ' shows a strong divergence $\chi' \sim T^{-1.2}$ in the magnetically easy plane, paired with an upturn in the imaginary susceptibility χ'' suggestive of ferromagnetism. Peaks near 2 K in χ', the specific heat C, and the resistivity ρ could signal a low-lying energy scale where a gap opens for the critical fluctuations associated with this incipient magnetic order. The unusually weak and itinerant magnetism in $CaMn_2Al_{10}$ appears to derive from strong Mn-Al hybridization, as revealed by density functional theory (DFT) calculations. With $T_c \leq 2$ K, $CaMn_2Al_{10}$ is the least stable itinerant Mn magnet known to date[40], and a prospective candidate to look for magnetically mediated superconductivity in a non-uranium based material. We note that there are very few known Mn-based superconductors, for instance pressurized MnP[41] and U_6Mn[42].

Single crystals of $CaMn_2Al_{10}$ were grown from self-flux, forming as square rods as large as 1 x 1 x 10 mm^3, where the crystallographic c-axis coincides with the rod axis. The crystal structure was determined from single crystal X-ray diffraction using a Bruker Apex II diffractometer, and the composition was verified by energy dispersive X-ray spectroscopy (EDS) using a JEOL 7600 F analytical scanning electron microscope. The temperature dependencies of the magnetic dc susceptibility $\chi(T)$ and ac susceptibility $\chi'(T)$ of an oriented single crystal were measured in the temperature range from 1.8 K $< T <$ 300 K using a Quantum Design Magnetic Properties Measurement System. The specific heat $C(T)$ and electrical resistivity $\rho(T)$ were measured in a Quantum Design Physical Properties Measurement System, down to 0.07 K or 0.4 K, respectively.

The crystal structure of $CaMn_2Al_{10}$ is visualized in Fig. 1, consisting of two Mn sublattices that form square plaquettes displaced along the c-axis. Our X-ray structure analysis, described in detail in[43], rules out the appreciable site disorder reported in other compounds forming in this and related structure-types[44–46]. Like YFe_2Al_{10}[47,48], $CaMn_2Al_{10}$ is stoichiometric and highly ordered. All Mn sites are equivalent, as shown in Fig. 1(a), with a nearest-neighbor Mn-Mn distance of 4.7 Å along the [110]-direction, and 5.1 Å along [001]. These minimum Mn-Mn spacings in $CaMn_2Al_{10}$ are well above the critical distance of 2.7 Å needed to suppress Mn moments, for instance in Laves phase compounds[18,49,50]. One would therefore expect localized Mn moments produced by strong Hund's interactions, although our results will show this is not the case.

Our measurements of the magnetic properties paint a rather different picture of the magnetism in $CaMn_2Al_{10}$, with strongly suppressed Mn moments and considerable low-T anisotropy. Fig. 2(a) shows the T dependence of $(\chi - \chi_0)^{-1}$ in a dc field $H = 1000$ Oe applied along the c-axis or in the ab-plane, respectively, where $\chi_0 = 3.2 \times 10^{-4}$ emu/mol Mn. In both cases, $\chi(T)$ obeys

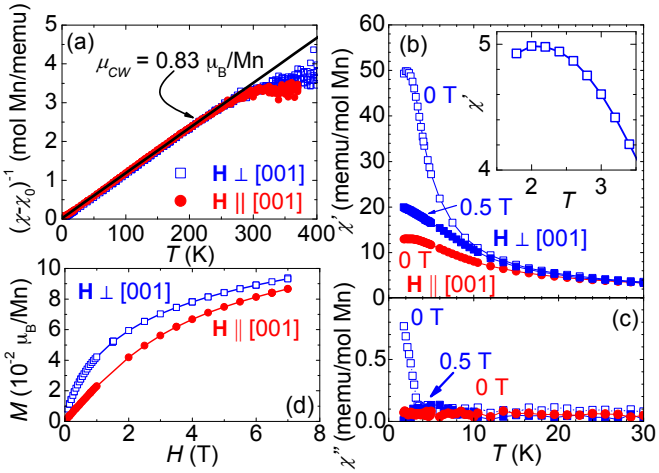

Figure 2. (Color online) (a) The T dependence of $(\chi - \chi_0)^{-1}$ measured with a 1000 Oe dc field $\mathbf{H} \parallel \mathbf{c}$ (red filled circles) and $\mathbf{H} \perp \mathbf{c}$(blue open squares). The solid black line is a fit to the CW law. (b) The T dependence of χ' with 4.17 Oe ac field and a dc field $\mathbf{H} \parallel \mathbf{c}$ of 0 T (red filled circles) and also $\mathbf{H} \perp \mathbf{c}$ of 0 T (blue open squares) and 0.5 T (blue filled squares). The inset shows a closeup of the maximum in the $\mathbf{H} \perp \mathbf{c} = 0$ T data. The solid lines serve as guides for the eye. (c) The temperature dependence of the imaginary part of the ac magnetic susceptibility χ'', colors as in (b). (d) The H dependence of the dc magnetization M, colors as indicated. The solid lines are guides for the eye.

the Curie Weiss (CW) law between 30 K and 300 K. The CW moments obtained from linear fits to $(\chi - \chi_0)^{-1}$ are $\mu_{CW} = 0.83 \pm 0.005\,\mu_B$/Mn for both orientations, while the Weiss temperatures are indistinguishable from zero. χ' (Fig. 2(b)) reveals a sizable anisotropy below 10 K, $\chi'_{[100]}/\chi'_{[001]} = 3.5$ for ac fields along [100] and [001]. We as well observe a peak in $\chi'(T)$ that is centered between 2-3 K (inset, Fig 2(b)), accompanied by a sharp increase in the imaginary susceptibility χ'' (Fig 2(c)). The dc magnetization $M(H)$, measured at 1.8 K with dc fields along these same directions, is nonlinear below 4 T and also displays a pronounced anisotropy that persists up to $H = 7$ T (Fig 2(d)). The Mn-moment $\mu_{CW} = 0.83\ \mu_B$/Mn obtained from CW fits is less than half of the moment $1.73\,\mu_B$ expected for the lowest-spin $s = 1/2$ configuration of Mn ions[51]. The magnitude of μ_{CW} and the pronounced anisotropy in $M(H,T)$ argue that their origin is intrinsic. These results are quantitatively reproduced in multiple samples, and both EDS and powder X-ray measurements show no indication of magnetic contaminants[43]. We therefore interpret this small but sizable μ_{CW} as a signature of itinerant magnetism in $CaMn_2Al_{10}$, supported by the slow approach to saturation observed in $M(H)$ (Fig. 2(d)). The observed magnetic anisotropy is unexpected in itinerant moment systems where single ion anisotropy is generally weak, and may reflect instead a 2D magnetic character with strong fluctuations in the magnetically easy ab-plane.

The peak in $\chi'(T)$ at 2 K and the steep increase in

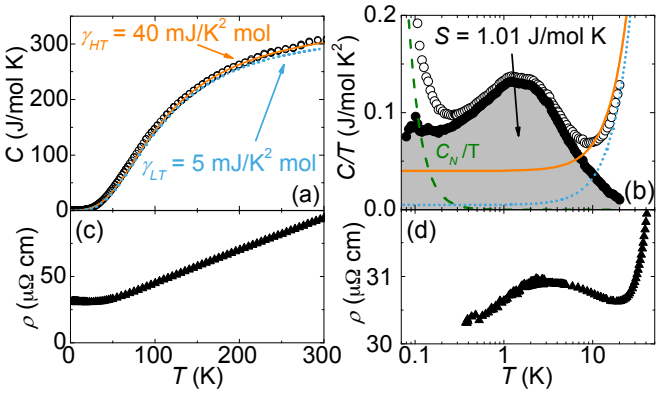

Figure 3. (Color online) (a) The temperature dependence of the specific heat C. The lines correspond to fits to the Debye model with $\gamma_{HT} = 40$ mJ/mol K^2 (orange solid) and $\gamma_{LT} = 5$ mJ/mol K^2 (blue dotted) as described in the text. (b) Plots of C/T (open black circles) and C_M/T (filled black circles, see text) versus T. The nuclear Schottky contribution C_N (green dashed line) and Debye contributions with γ_{HT} (orange solid line) and γ_{LT} (blue dotted line) are overplotted. The entropy S (see text) is shaded gray. (c) The temperature dependence of the resistivity ρ, with current flowing along the c-axis. (d) A semi-log plot of $\rho(T)$.

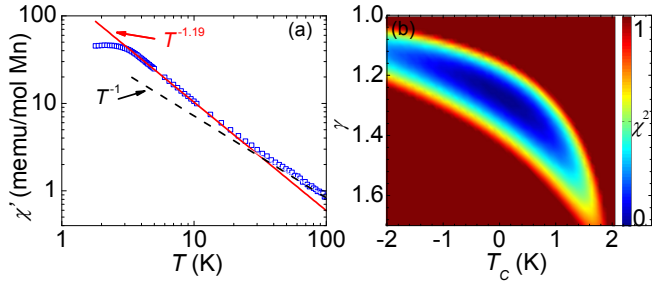

Figure 4. (Color online) (a) The temperature dependence of the real part of the ac susceptibility χ' (blue open squares). The solid red line is a fit to $\chi' \sim (T - T_C)^{-\gamma}$ as described in the text. The dashed black line corresponds to the CW fit in Fig. 2(a). (b) The mean square deviation χ^2 for fit parameters γ and T_C.

$\chi''(T)$ suggest a new energy scale at low temperatures, possibly related to magnetic order, which is evident in other physical properties as well. To clarify the origin of these anomalies, we measured the specific heat $C(T)$, shown in Fig. 3 (a),(b). Above $T \approx 20$ K, $C(T)$ is well described by a Debye model with Debye temperature $\theta_D = 450$ K, representing the lattice contribution $C_L(T)$, and a Sommerfeld coefficient $\gamma_{HT} = 40$ mJ/mol K^2 for the electronic component. A different model is required for $T < 20$ K, where a reduced $\gamma_{LT} = 5$ mJ/mol K^2 gives a better estimate of the electronic specific heat (Fig. 3(b)). Below 0.5 K, $C(T)$ is increasingly dominated by a diverging contribution that we attribute to a nuclear Schottky effect $C_N(T)$ of the Mn atoms. Accordingly, this tail is well fitted by the expression $C_N(T)$=a/T^2 (Fig. 3b). The magnetic specific heat is obtained as $C_M(T) = C(T) - C_N(T) - C_L(T) - \gamma_{LT}T$. $C_M(T)/T$ approaches a constant value of 80 mJ/mol K^2 at the lowest temperatures, much higher than $\gamma_{LT} = 5$ mJ/mol K^2. If this large specific heat at low T stems from the conduction electron system, it indicates a significant change in the Fermi surface volume and strong correlations below 2 K. The most prominent feature of $C(T)$ is a broad peak, whose maximum occurs near the same temperature $\simeq$2 K as the peak found in χ' (inset, Fig. 2(b)). Integrating $C_M(T)/T$ over T yields an entropy of $S = 1.01 \pm 0.02$ J/K mol formula unit. This corresponds to only 9 % of the entropy difference $\Delta S = R \ln 2 = 5.76$ J/mol Mn K[52] expected for full ordering of localized moments on the Mn sites with the smallest possible spin $s = 1/2$. This small entropy is consistent with itinerant magnetism inferred from the magnetic properties.

Further evidence for a new energy scale emerging at the lowest temperatures comes from the electrical resistivity $\rho(T)$, which is metallic with a linear T-dependence above ≈ 20 K (Fig. 3c). A close-up (Fig. 3(d)) reveals a weak peak in $\rho(T)$ around 2-3 K, coinciding with the anomalies in $\chi'(T)$ (Fig. 2(b)) and $C(T)$ (Fig. 3(b)). Meanwhile, the minimum and upturn in ρ around 20 K, shown in Fig. 3(d), is concurrent with the apparent reduction of the Sommerfeld coefficient below 20 K, also suggesting a Fermi surface instability.

The strongest evidence for incipient magnetic order comes from $\chi'(T)$ and $\chi''(T)$, measured with the field in the magnetically easy ab - plane. Fig. 4(a) shows a double-logarithmic plot of $\chi'(T)$ at low temperatures. Two different regimes can be distinguished: a CW-like behavior above 30 K, and a stronger divergence for 3.5 K $\leq T \leq$ 20 K. While this range of temperatures is limited, due to the apparent saturation at the lowest T, Fig. 4(a) and the analysis in Fig. 4(b) show that these data diverge more strongly than the CW expression, consistent with a power law $\chi'(T) \sim (T - T_C)^{-\gamma}$ with $\gamma = 1.19 \pm 0.07$ and $T_C = 0.1 \pm 0.3$ K. This observation of $\gamma > 1$ is significant, as it implies that we can exclude impurities as the origin of the diverging susceptibility[53,54], as well as disorder driven mechanisms such as a Griffiths phase[55], where $C(T)$ and $\chi'(T)$ both diverge as $T^{\lambda-1}$ as $T \to T_C$, and where $0 \leq \lambda \leq 1$. While it is clear that the susceptibility upturn signals proximity to magnetic order, mostly likely with a FM component, the unknown impact of magnetocrystalline anisotropy[35,36,56] cautions against attributing it entirely to the critical fluctuations associated with a $T = 0$ magnetic transition. However, it is intriguing that the value of $\gamma \sim 1.2$ taken from the least squres fit is rather close to $\gamma = 4/3$, which is the value given by the Hertz-Millis-Moriya mean field theory of the 2D metallic FM[57–59]. Since the divergence of the susceptibility is cut off for $T < 2$ K, $CaMn_2Al_{10}$ may still need to be tuned compositionally or by applying pressure to become truly critical at $T = 0$.

Hund's rule leads to local moments as large as 5 μ_B in

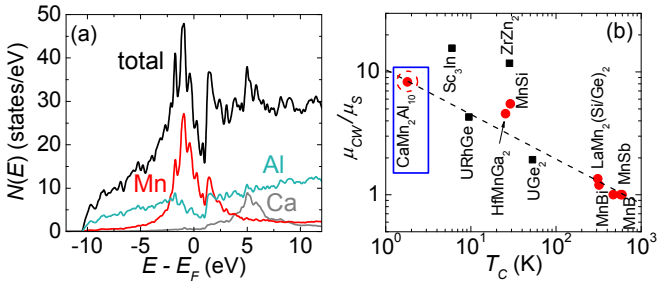

Figure 5. (Color online) (a) The total (black), Mn (red), Al (teal), and Ca (gray) density of states $N(E)$ as indicated. (b) A Rhodes-Wohlfarth plot of μ_{CW}/μ_S versus T_C for FM materials, with Mn-based compounds shown in red. The placement of $CaMn_2Al_{10}$ on the guide for the eye (dashed line) is described in the text. Data from[10,11,17,19,25–27,31].

the $3d^5$ Mn^{2+} state, so why is the magnetic moment in $CaMn_2Al_{10}$ so small? To address this question, we have calculated the density of states using density-functional theory with generalized gradient approximation potential[60] implemented in the WIEN2k all-electron scheme[61]. Spin polarized calculations for the FM state reveal a magnetic moment of $0.9\,\mu_B$ on the Mn site, which is close to the observed CW moment of $0.83\,\mu_B$. As shown in Fig. 5(a), the Fermi surface is associated with bands derived predominantly from Mn $3d$-electrons. These are strongly hybridized with Al $3s$ and $3p$ states, effectively quenching the majority of the Mn moment. The hybridization opens a pronounced pseudogap at the Fermi surface, which has been shown to be responsible for the stabilization of complex Mn-Al alloys[62]. This stabilization mechanism favors a Mn-Mn spacing of 4.7 Å[63] - just as in $CaMn_2Al_{10}$. Despite the long Mn-Mn distance, we conclude that the weak itinerant magnetism in $CaMn_2Al_{10}$ is the consequence of strong Mn-Al hybridization.

The emerging picture of $CaMn_2Al_{10}$ is as a system on the verge of itinerant moment order, and the strong divergence of $\chi'(T)$ suggests that FM, or at least a FM component, is most likely. Accordingly, we tentatively place $CaMn_2Al_{10}$ on the phenomenological Rhodes-Wohlfarth (RW) curve[64] for FM (Fig. 5(b)), which relates the ratio of fluctuating and saturation moments μ_{CW}/μ_S to T_C. Since our measurements constrain T_C to be less than 2 K, $CaMn_2Al_{10}$ appears on the extreme left of the RW curve, where it is neighbored mostly by itinerant U-based compounds with $\mu_{CW} >> \mu_S$. $CaMn_2Al_{10}$ appears to be distinct, however, from many of these previously known FM, since our susceptibility measurements infer a fluctuating moment that is even more reduced from the free ion value. With T_C constrained to ≤ 2 K, the RW curve predicts $\mu_{CW}/\mu_S \geq 8$ for $CaMn_2Al_{10}$. If it does indeed order ferromagnetically, this ratio, combined with the small fluctuating moment we calculate from $\chi(T)$, yields a spontaneous moment $\mu_S \leq 0.1\ \mu_B$, some two orders of magnitude smaller than the high spin Hund's rule value and consistent with the value of $M(H)$ at 7 T. Perhaps $CaMn_2Al_{10}$ is most comparable to Sc_3In, which has an ordered moment of only 0.04-0.05 μ_B[65]. Considering that Mn-based compounds are generally strongly magnetic, while those based on Sc are nearly always nonmagnetic, both Sc_3In and $CaMn_2Al_{10}$ appear as remarkable and extreme members even among weak itinerant magnets. The strong hybridization, that suppresses the magnetic moments and limits magnetic order to a vanishingly low temperature, makes $CaMn_2Al_{10}$ unique for a magnetic Mn-based compound. While we can not yet say for certain if the experimental features we observe are the hallmarks of magnetic order or only impending magnetic order, in either case the ordering temperature would be remarkably low, and quantum critical fluctuations may potentially be present, as in the related 2D-quantum critical FM YFe_2Al_{10}[35].

ACKNOWLEDGMENTS

Work at Brookhaven National Laboratory was carried out under the auspices of US Department of Energy, Office of Basic Energy Sciences, Contract DE-AC02-98CH1886. Research carried out in part at the Center for Functional Nanomaterials, Brookhaven National Laboratory, was supported by the U.S. Department of Energy, Office of Basic Energy Sciences, under Contract No. DE-SC0012704.

*lsteinke@bnl.gov

[1] A. Georges, L. de' Medici and J. Mravlje, Annu. Rev. Condens. Matter Phys. **4** (2013) 137-78.
[2] D. A. Young, *Phase Diagrams of the Elements*, Berkeley, Los Angeles, CA: University of California Press (1991).
[3] D. Hobbs, J. Hafner, and D. Spišák, Phys. Rev. B **68**, 014407 (2003).
[4] J. W. Simonson, Z. P. Yin, M. Pezzoli, J. Guo, J. Liu, K. Post, A. Efimenko, N. Hollman, Z. Hu, H.-J. Lin, C.-T. Chen, C. Marques, V. Leyva, G. Smith, J. W. Lynn, L. L. Sun, G. Kotliar, D. N. Basov, L. H. Tjeng, and M. C. Aronson, Proc. Natl. Acad. Sci. U.S.A. **109**, E1815 (2012).
[5] D. E. McNally, J. W. Simonson, K. W. Post, Z. P. Yin, M. Pezzoli, G. J. Smith, V. Leyva, C. Marques, L. DeBeer-Schmitt, A. I. Kolesnikov, Y. Zhao, J. W. Lynn, D. N. Basov, G. Kotliar, and M. C. Aronson, Phys. Rev. B **90**, 180403(R) (2014).
[6] J. W. Simonson, G. J. Smith, K. Post, M. Pezzoli, J. J. Kistner-Morris, D. E. McNally, J. E. Hassinger, C. S. Nelson, G. Kotliar, D. N. Basov, and M. C. Aronson, Phys. Rev. B **86**, 184430 (2012).
[7] D. E. McNally, J. W. Simonson, J. J. Kistner-Morris, G. J. Smith, J. E. Hassinger, L. DeBeer-Schmitt, A. I.

Kolesnikov, I. A. Zaliznyak, and M. C. Aronson, Phys. Rev. B **91**, 180407(R) (2015).
[8] D. C. Johnston, R. J. McQueeney, B. Lake, A. Honecker, M. E. Zhitomirsky, R. Nath, Y. Furukawa, V. P. Antropov, and Yogesh Singh, Phys. Rev. B. **84**, 094445 (2011).
[9] E. E. Huber, Jr. and D. H. Ridgley, Phys. Rev. **135**, A1033 (1964).
[10] R. R. Heikes, Phys. Rev. B **99**, 446 (1955).
[11] K. Ahlborn, K. Bärner, and W. Schröter, phys. stat. sol. (a) **30**, 251 (1975).
[12] S. Hilpert and T. Diekmann, Ber. Deutsche Chem. Gesellsch. A **44**, 2378 (1911).
[13] N. Lundquist and H. P. Myers, Ark. Fys **20**, 463 (1961).
[14] T. Shigeoka, N. Iwata, H. Fujii, and T. Okamoto, J. Magn. Magn. Mater. **53**, 83 (1985).
[15] A. Szytuła, J. Leciejewicz, *Handbook of Crystal Structures and Magnetic Properties of Rare Earth Intermetallics*, CRC Press, Boca Raton, FL (1994).
[16] S. Okada, K. Kudou, T. Mori, K. Iizumi, T. Shishido, T. Tanaka, and P. Rogl, J. Crys. Growth **244**, 267 (2002).
[17] H. J. Williams, J. H. Wernick, R. C. Sherwood, and G. K. Wertheim, J. Appl. Phys. **37**, 1256 (1966)., J. H. Wernick, G. K. Wertheim, and R. C. Sherwood, Mater. Res. Bull. **7**, 1431 (1972).
[18] M. Shiga, Physica B **149**, 293 (1988).
[19] C. Marques, Y. Janssen, M. S. Kim, L. Wu, S. X. Chi, J. W. Lynn, and M. C. Aronson, Phys. Rev. B **83**, 184435 (2011).
[20] E. C. Stoner, Proc. R. Soc. London A **165**, 372 (1938).
[21] E. Fawcett, H. L. Alberts, V. Yu. Galkin, D. R. Noakes, and J. V. Yakhmi, Rev. Mod. Phys. **66**, 25 (1994).
[22] T. Moriya, it Spin fluctuations in Itinerant Electron Magnetism Springer, New York (1985).
[23] G. G. Lonzarich and L. Taillefer, J. Phys. C. **18**, 4339 (1985).
[24] C. Pfleiderer, Rev. Mod.. Phys. **81**, 1551 (2009).
[25] B. T. Matthias, A. M. Clogston, H. J. Williams, E. Corenzwit, and R. C. Sherwood, Phys. Rev. Lett. **7**, 7 (1961).
[26] D. Aoki, A. Huxley, E. Ressouche, D. Braithwaite, J. Flouquet, J.-P. Brison, E. Lhotel, C. Paulsen, Nature **413**, 613 (2001).
[27] S. S. Saxena, P. Agarwal, K. Ahilan, F. M. Grosche, R. K. W. Haselwimmer, M. J. Steiner, E. Pugh, I. R. Walker, S. R. Julian, P. Monthoux, G. G. Lonzarich, A. Huxley, I. Sheikin, D. Braithwaite, and J. Flouquet, Nature **406**, 587 (2000).
[28] J. H. Fluitman, B. R. de Vries, R. Boom, and C. J. Schinkel, Phys. Lett. A **28**, 506 (1969).
[29] C. Pfleiderer, M. Uhlarz, S. M. Hayden, R. Vollmer, H. v. Löhneysen, N. R. Bernhoeft, and G. G. Lonzarich, Nature **412**, 58 (2001).
[30] D. A. Sokolov, M. C. Aronson, W. Gannon, and Z. Fisk, Phys. Rev. Lett. **96**, 116404 (2006).
[31] B. T. Matthias and R. M. Bozorth, Phys. Rev. **109**, 604 (1958).
[32] D. Belitz, T. R. Kirkpatrick, and T. Vojta, Rev. Mod. Phys. **77**, 579 (2005).
[33] C. Pfleiderer, G. J. McMullan, S. R. Julian, and G. G. Lonzarich, Phys. Rev. B **55**, 8330 (1997).
[34] M. Uhlarz, C. Pfleiderer, and S. M. Hayden, Phys. Rev. Lett. **93**, 256404 (2004).
[35] L. S. Wu, M. S. Kim, K. Park, A. M. Tsvelik, and M. C. Aronson, Proc. Natl. Acad. Sci. USA **111**, 14088 (2014).
[36] A. Steppke, R. Küchler, S. Lausberg, E. Lengyel, L. Steinke, R. Borth, T. Lühmann, C. Krellner, M. Nicklas, C. Geibel, F. Steglich, and M. Brando, Science **339**, 933 (2013).
[37] Z. Huesges, M. M. Koza, J. P. Embs, T. Fennell, G. Simeoni, C. Geibel, C. Krellner, and O. Stockert, J. Phys.: Conf. Ser. **592**, 012083 (2015).
[38] T. Akazawa, H. Hidaka, H. Kotegawa, T. C. Kobayashi, T. Fujiwara, E. Yamamoto, Y. Haga, R. Settai, and Y. Onuki, Physica B **359-361**, 1138 (2005).
[39] N. T. Huy, A. Gasparini, D. E. de Nijs, Y. Huang, J. C. P. Klaasse, T. Gortenmulder, A. de Vissier, A. Hamann, T. Gorlach, and H. v. Löhneysen, Phys. Rev. Lett. **99**, 067006 (2007).
[40] The AFM YMn_2 (T_N = 100 K)[18] and the FM MnSi (T_C = 29.1 K)[17] and $HfMnGa_2$ (T_C = 25.6 K)[19] all order at significantly higher temperatures than $CaMn_2Al_{10}$.
[41] J.-G. Cheng, K. Matsubayashi, W. Wu, J. P. Sun, F. K. Lin, J. L. Luo, and Y. Uwatoko, Phys. Rev. Lett. **114**, 117001 (2015).
[42] J. J. Engelhardt, J. Phys. Chem. Solids **36**, 123 (1975).
[43] See Supplemental Material at [URL will be inserted by publisher] for details of the X-ray structural analysis.
[44] V. M. Thiede, W. Jeitschko, Z. Naturforsch. **53 b**, 673 (1998).
[45] A. S. Sefat, S. L. Bud'ko, and P. C. Canfield, Phys. Rev. B **79**, 174429 (2009).
[46] B. F. Fulfer, N. Haldolaarachchige, D. P. Young, and J. Y. Chan, J. Solid State Chem. **194**, 143 (2012).
[47] K. Park, L. S. Wu, Y. Janssen, M. S. Kim, C. Marques, and M. C. Aronson, Phys. Rev. B **84**, 094425 (2011).
[48] A. Kerkau, L. Wu, K. Park, Y. Prots, M. Brando, M. C. Aronson, and G. Kreiner, Z. Kristallogr. NCS **227**, 289 (2012).
[49] H. Wada, H. Nakamura, K. Yoshimura, M. Shiga, and Y. Nakamura, J. Magn. Magn. Mater. **70**, 134 (1987).
[50] N. H. Kim-Ngan, P. E. Brommer, and J. J. M. Franse, IEEE Trans. Magn. **30(2)**, 837 (1994).
[51] N. Goldenberg, Trans. Faraday Soc. **36**, 847 (1940).
[52] The factor of 2 accounts for two Mn sites per formula unit of $CaMn_2Al_{10}$.
[53] B. Andraka and A. M. Tsvelik, Phys. Rev. Lett. **67**, 2886 (1991).
[54] A. M. Tsvelik and M. Reizer, Phys. Rev. B **48**, 9887 (1993).
[55] T. Vojta, J. Low Temp. Phys. **161**, 299 (2010).
[56] W. Fernengel, H. Kronm—"uller, J. Magn. Magn. Mater. **13**, 211 (1079).
[57] J. A. Hertz, Phys. Rev. B **14**, 1165 (1976).
[58] T. Moriya, Springer Series in Solid-State Sciences, Vol. **56** Springer, Berlin (1985).
[59] A. J. Millis, Phys. Rev. B **48**, 7183 (1993).
[60] J. P. Perdew , K. Burke , M. Ernzerhof , Phys. Rev. Lett. **77**, 3865 (1996).
[61] P. Blaha, K. Schwarz, G. K. H. Madsen, D. Kvasnicka, and J. Luitz, ***WIEN2k****, An Augmented Plane Wave + Local Orbitals Program for Calculating Crystal Properties* (Karlheinz Schwarz, Techn. Universität Wien, Austria), 2001. ISBN 3-9501031-1-2. We used version 14.1 with default recommended parameters. The Brillouin zone was sampled with a $11\times11\times29$ mesh to achieve energy convergence of 1 meV; increasing the k-mesh to $24\times24\times60$ does not introduce noticeable changes in the density of states shown in Fig. 5(b).
[62] U. Häussermann, P. Viklund, M. Boström, R. Norrestam, and S. I. Simak, Phys. Rev. B **63**, 125118 (2001).

[63] J. Zou and A. E. Carlsson, Phys. Rev. Lett. **70**, 3748 (1993).
[64] P. R. Rhodes and E. P. Wolfarth, Proc. Roy. Soc. **273**, 247 (1963).
[65] K. Kamishima, R. Note, T. Imakubo, K. Watanabe, H. A. Katori, A. Fujimori, M. Sakai, and K. V. Kamenev J. Alloys and Compd. **589**, 37-41 (2014).